Nonlinear Dyn (2015) 81:1247–1262
DOI 10.1007/s11071-015-2065-6

ORIGINAL PAPER

A new lattice hydrodynamic model for bidirectional pedestrian flow with the consideration of pedestrian's anticipation effect

Jie Zhou · Zhong-Ke Shi

Received: 5 October 2014 / Accepted: 29 March 2015 / Published online: 8 April 2015

Abstract Considering the effect of pedestrian's anticipation, an extended lattice hydrodynamic model for bidirectional pedestrian flow with passing is proposed in this paper. The stability condition is obtained by the use of linear stability analysis. It is shown that the anticipation term can significantly enlarge the stability region on the phase diagram, and the passing term may reduce the stability region and aggravate the pedestrian jam. Based on nonlinear analysis method, the Burgers, Korteweg–de Vries and modified Korteweg–de Vries equations are derived to describe the shock waves, soliton waves and kink–antikink waves in the stable, metastable and unstable region, respectively. The theoretical results show that jams may be alleviated efficiently by considering the effect of pedestrian's anticipation. Numerical simulations are carried out in order to verify the theoretical results.

Keywords Pedestrian flow · Nonlinear analysis · Anticipation · MKdV equation

J. Zhou
School of Mathematics, Physics and Information Science, Zhejiang Ocean University, Zhoushan 316000, China

J. Zhou
Key Laboratory of Oceanographic Big Data Mining & Application of Zhejiang Province, Zhejiang Ocean University, Zhoushan 316022, China

J. Zhou (✉) · Z.-K. Shi
College of Automation, Northwestern Polytechnical University, Xi'an 210097, Shanxi, China
e-mail: zhoujie@zjou.edu.cn

1 Introduction

In recent years, with the development of urbanization, pedestrian flow becomes a topic issue in public security problems. The congested pedestrian flow not only causes much inconvenience, but also results in security risks for pedestrian. Pedestrian flow has attracted considerable attention in the field of physical science [1–6]. In order to gain a better understanding of pedestrian flow, there is a demand for realistic and quantitative models that can predict pedestrian movements and travel times for a given infrastructure and duplicate the phenomena observed in real situation. To achieve this goal, various pedestrian flow models including the social force models, the hydrodynamic models, the cellular automaton models, the lattice models and emergency and evacuation models were proposed by many scholars with different backgrounds. A series of experiments had been done for investigating the mechanism of pedestrian flow and identifying the influence factors. Many interesting nonequilibrium phenomena such as phase transition, density waves, freezing by heating and faster-is-slow effect in panic situations, sudden transitions from laminar to stop-and-go and turbulent flows had been observed. To investigate and represent the complex phenomena of pedestrian flow, investigations have been carried out by scholars using different methodologies [7–32], such as mathematical modeling and simulation, experimental studies. Compared with experimental studies, mathematical modeling and simulation have the ability to study pedestrian flow in

general and get the analytical results easily. Dynamical models for pedestrian flow are useful for such studies, especially for analytical studies, because the motion of pedestrians is described by the dynamical equation of motion [27].

Pedestrian flow dynamics is similar to the traffic flow dynamics to some extent. Ivancevic and Reid [23] analyzed crowd turbulence from both classical and quantum perspective and found shock waves and soliton waves in crowd dynamics. The nonlinear waves in traffic dynamics have been investigated by using nonlinear analysis [33–41]. Kerner et al. [33] had found the single-pulse density waves in the numerical simulation with the hydrodynamic model. Kurtze and Hong [34] had shown that the single-pulse density wave is a soliton. Komatsu and Sasa [35] derived MKdV equation from optimal velocity model to describe the traffic jams in terms of the kink density waves. In pedestrian flow theory, based on the two-dimensional optimal velocity model proposed by Nakayama et al. [27,28], Tian et al. [19] proposed a new lattice hydrodynamic model for bidirectional pedestrian flow and derived the MKdV equations to describe the density wave of pedestrian congestion. Considering the pedestrian's visual field effects, Kuang et al. [13] proposed an extended lattice hydrodynamic model for bidirectional pedestrian flow and concluded that taking the pedestrian's visual field effect into account can improve the stability of pedestrian flow dynamics.

Anticipation effect, which is considered as pedestrian's ability of avoiding collisions by forecasting other pedestrians movement, adjusting their velocity according to the observed surrounding situations and estimating their walking behavior, plays an important role in stabilizing and destabilizing the pedestrian flow. Heavy jamming and confusion would occur if no one should anticipate, especially under crowded situations. In Ref. [42], considering the anticipation as the ability of avoiding collisions with other pedestrians, Suma et al. proposed the anticipation floor field (AFF) as an extension of the floor field (FF) model and found that strength and range of anticipation significantly affect pedestrian dynamics. However, the effect of pedestrian's anticipation on the formation mechanism of density wave of pedestrian jam has not been considered. In this paper, taking the effect of pedestrian's anticipation into account, an extended lattice hydrodynamic model for bidirectional pedestrian flow with passing is proposed.

The paper is organized as follows. In Sect. 2, the model is formulated by considering anticipation effect and passing effect. The stability analysis is obtained by using linear stability analysis in Sect. 3. We can see the stability condition varies with the anticipation effect. In Sect. 4, the Burgers, KdV and MKdV equations are derived in three types of pedestrian flow regions by using nonlinear analysis. Numerical simulations are given in Sect. 5.

2 Model

In this section, considering the effect of pedestrian's anticipation in pedestrian dynamics with passing, an extended lattice hydrodynamic model for bidirectional pedestrian flow will be established. As mentioned in Ref. [19], in the two-dimensional bidirectional pedestrian flow, four types of pedestrians are considered: east-bound pedestrians move freely only to the positive x direction $x+$, west-bound only to the negative x direction $x-$, north-bound only to the positive y direction $y+$, and south-bound only to the negative y direction $y-$. Figure 1 is the illustration of the two-dimensional bidirectional pedestrian flow.

The continuity equations of the east-bound, west-bound, north-bound and south-bound pedestrians are given as follows [19]

$$\partial_t \rho_{x+}(j,m,t) + cc_1\rho_0[Q_{x+}(j,m,t) - Q_{x+}(j-1,m,t)] = 0, \quad (1)$$

$$\partial_t \rho_{x-}(j,m,t) + c(1-c_1)\rho_0[Q_{x-}(j,m,t) - Q_{x-}(j+1,m,t)] = 0, \quad (2)$$

$$\partial_t \rho_{y+}(j,m,t) + (1-c)c_2\rho_0[Q_{y+}(j,m,t) - Q_{y+}(j,m-1,t)] = 0, \quad (3)$$

$$\partial_t \rho_{y-}(j,m,t) + (1-c)(1-c_2)\rho_0[Q_{y-}(j,m,t) - Q_{y-}(j,m+1,t)] = 0, \quad (4)$$

where ρ_0 is the total average density, $\rho_{x+}(x,y,t)$, $\rho_{x-}(x,y,t)$, $\rho_{y+}(x,y,t)$, $\rho_{y-}(x,y,t)$ denote the density of east-bound, west-bound, north-bound and south-bound pedestrians at site (x,y) at time t, respectively, and $Q_{x+}(x,y,t)$, $Q_{x-}(x,y,t)$, $Q_{y+}(x,y,t)$, $Q_{y-}(x,y,t)$ represent the flux of east-bound, west-bound, north-bound and south-bound pedestrians at site (x,y) at time t, respectively. c is the proportion of east-bound and west-bound pedestrians in all pedestrians,

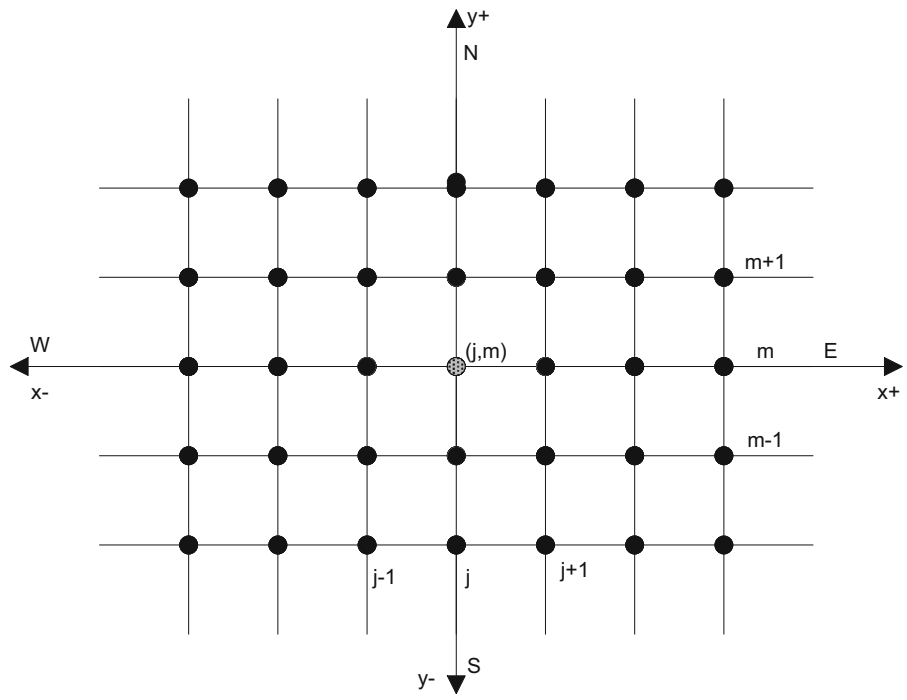

Fig. 1 The schematic diagram of the moving direction of the pedestrians when n sites in front of site (j, m) are considered. The circle denotes the position of site, and E, W, N and S represent the east-bound, west-bound, north-bound, and south-bound pedestrians, respectively.

c_1 is the proportion of east-bound pedestrians in east-bound and west-bound pedestrians, and c_2 is the proportion of north-bound pedestrians in north-bound and south-bound pedestrians.

In terms of Nagatani's idea [25], the flux for each direction pedestrian is determined by the total optimal current with delay time τ, that is [19]

$$Q_{x+}(j,m,t+\tau) = cc_1\rho_0 V(\rho(j+1,m,t)), \tag{5}$$

$$Q_{x-}(j,m,t+\tau) = c(1-c_1)\rho_0 V(\rho(j-1,m,t)), \tag{6}$$

$$Q_{y+}(j,m,t+\tau) = (1-c)c_2\rho_0 V(\rho(j,m+1,t)), \tag{7}$$

$$Q_{y-}(j,m,t+\tau) = (1-c)(1-c_2)\rho_0 V(\rho(j,m-1,t)). \tag{8}$$

Here, $V(\rho(j,m,t))$ is the optimal velocity function and adopted as in Ref. [25], that is

$$V(\rho(j,m,t)) = \tanh\left(\frac{2}{\rho_0} - \frac{\rho(j,m,t)}{\rho_0^2} - \frac{1}{\rho_c}\right) + \tanh\left(\frac{1}{\rho_c}\right). \tag{9}$$

where ρ_c is the critical density and it is equal to the inverse of the safety distance [26].

Considering the effect of pedestrian's anticipation on the pedestrian flow with passing, we extend the flux for each direction pedestrian based on Nagatani's idea [43]

$$\begin{aligned} Q_{x+}(j,m,t+\tau) &= cc_1\rho_0 V(\rho(j+1,m,t+\alpha\tau)) \\ &\quad + \lambda cc_1\rho_0[V(\rho(j+1,m,t+\alpha\tau)) \\ &\quad - V(\rho(j+2,m,t+\alpha\tau))], \end{aligned} \tag{10}$$

$$\begin{aligned} Q_{x-}(j,m,t+\tau) &= c(1-c_1)\rho_0 V(\rho(j-1,m,t+\alpha\tau)) \\ &\quad + \lambda c(1-c_1)\rho_0[V(\rho(j-1,m,t+\alpha\tau)) \\ &\quad - V(\rho(j-2,m,t+\alpha\tau))], \end{aligned} \tag{11}$$

$$\begin{aligned} Q_{y+}(j,m,t+\tau) &= (1-c)c_2\rho_0 V(\rho(j,m+1,t+\alpha\tau)) \\ &\quad + \lambda(1-c)c_2\rho_0[V(\rho(j,m+1,t+\alpha\tau)) \\ &\quad - V(\rho(j,m+2,t+\alpha\tau))], \end{aligned} \tag{12}$$

$$\begin{aligned} Q_{y-}(j,m,t+\tau) &= (1-c)(1-c_2)\rho_0 \\ &\quad \times V(\rho(j,m-1,t+\alpha\tau)) \\ &\quad + \lambda(1-c)(1-c_2) \\ &\quad \times \rho_0[V(\rho(j,m-1,t+\alpha\tau)) \\ &\quad - V(\rho(j,m-2,t+\alpha\tau))], \end{aligned} \tag{13}$$

where λ is the reaction coefficient to the passing effect and $\alpha > 0$ represents anticipation walking behavior or the pedestrian's forecast effect in a pedestrian dynamics. And the bigger value of α corresponds to conscious pedestrian in the model.

Inserting Eqs. (10)–(13) into Eqs. (1)–(4) and using

$$\begin{aligned} \rho(j,m,t) &= \rho_{x+}(j,m,t) + \rho_{x-}(j,m,t) \\ &\quad + \rho_{y+}(j,m,t) + \rho_{y-}(j,m,t), \end{aligned}$$

the total density equation is obtained as

$$\begin{aligned}
&\rho(j,m,t+2\tau)-\rho(j,m,t+\tau)+\tau(cc_1\rho_0)^2\\
&\quad[V(\rho(j+1,m,t+\alpha\tau))-V(\rho(j,m,t+\alpha\tau))]\\
&\quad+\tau[c(1-c_1)\rho_0]^2[V(\rho(j-1,m,t+\alpha\tau))\\
&\quad-V(\rho(j,m,t+\alpha\tau))]+\tau[(1-c)c_2\rho_0]^2\\
&\quad[V(\rho(j,m+1,t+\alpha\tau))-V(\rho(j,m,t+\alpha\tau))]\\
&\quad+\tau[(1-c)(1-c_2)\rho_0]^2\\
&\quad[V(\rho(j,m-1,t+\alpha\tau))-V(\rho(j,m,t+\alpha\tau))]\\
&\quad+\lambda\tau(cc_1\rho_0)^2[2V(\rho(j+1,m,t+\alpha\tau))\\
&\quad-V(\rho(j+2,m,t+\alpha\tau))-V(\rho(j,m,t+\alpha\tau))]\\
&\quad+\lambda\tau[c(1-c_1)\rho_0]^2[2V(\rho(j-1,m,t+\alpha\tau))\\
&\quad-V(\rho(j-2,m,t+\alpha\tau))-V(\rho(j,m,t+\alpha\tau))]\\
&\quad+\lambda\tau[(1-c)c_2\rho_0]^2[2V(\rho(j,m+1,t+\alpha\tau))\\
&\quad-V(\rho(j,m+2,t+\alpha\tau))-V(\rho(j,m,t+\alpha\tau))]\\
&\quad+\lambda\tau[(1-c)(1-c_2)\rho_0]^2[2V(\rho(j,m-1,t+\alpha\tau))\\
&\quad-V(\rho(j,m-2,t+\alpha\tau))-V(\rho(j,m,t+\alpha\tau))]=0.
\end{aligned}\tag{14}$$

3 linear stability analysis

We apply the linear stability theory to analyze the pedestrian flow model described by Eq. (14). Supposing the pedestrian running with the uniform density ρ_0 and optimal velocity $V(\rho_0)$ along four directions, then we get the uniform steady-state solution $\rho(j,m,t)$ for Eq. (14)

$$\begin{aligned}
&\rho(j,m,t)=\rho_0,\\
&v_{x+}(j,m,t)=v_{x-}(j,m,t)\\
&=v_{y+}(j,m,t)=v_{y-}(j,m,t)=V(\rho_0).
\end{aligned}\tag{15}$$

Assuming $y(j,m,t)$ be a small deviation from the uniform steady solution, that is

$$\rho(j,m,t)=\rho_0+y(j,m,t).\tag{16}$$

Inserting it and Eq. (15) into Eq. (14), then the linearized equation for $y(j,m,t)$ is obtained from Eq. (14)

$$\begin{aligned}
&y(j,m,t+2\tau)-y(j,m,t+\tau)\\
&\quad+\tau(cc_1\rho_0)^2V'(\rho_0)[y(j+1,m,t+\alpha\tau)\\
&\quad-y(j,m,t+\alpha\tau)]\\
&\quad+\tau[c(1-c_1)\rho_0]^2V'(\rho_0)[y(j-1,m,t+\alpha\tau)\\
&\quad-y(j,m,t+\alpha\tau)]\\
&\quad+\tau[(1-c)c_2\rho_0]^2V'(\rho_0)[y(j,m+1,t+\alpha\tau)\\
&\quad-y(j,m,t+\alpha\tau)]\\
&\quad+\tau[(1-c)(1-c_2)\rho_0]^2V'(\rho_0)\\
&[y(j,m-1,t+\alpha\tau)-y(j,m,t+\alpha\tau)]\\
&\quad+\lambda\tau(cc_1\rho_0)^2V'(\rho_0)\\
&[2y(j+1,m,t+\alpha\tau)-y(j+2,m,t+\alpha\tau)\\
&\quad-y(j,m,t+\alpha\tau)]\\
&\quad+\lambda\tau[c(1-c_1)\rho_0]^2V'(\rho_0)\\
&[2y(j-1,m,t+\alpha\tau)-y(j-2,m,t+\alpha\tau)\\
&\quad-y(j,m,t+\alpha\tau)]\\
&\quad+\lambda\tau[(1-c)c_2\rho_0]^2V'(\rho_0)\\
&[2y(j,m+1,t+\alpha\tau)-y(j,m+2,t+\alpha\tau)\\
&\quad-y(j,m,t+\alpha\tau)]\\
&\quad+\lambda\tau[(1-c)(1-c_2)\rho_0]^2V'(\rho_0)\\
&[2y(j,m-1,t+\alpha\tau)-y(j,m-2,t+\alpha\tau)\\
&\quad-y(j,m,t+\alpha\tau)]\\
&=0,
\end{aligned}\tag{17}$$

where $V'(\rho_0)$ is the derivative of optimal velocity function $V(\rho)$ at point $\rho=\rho_0$. Expand $y(j,m,t)\propto\exp[ik(j+m)+zt]$ resulting in the following equation of z

$$\begin{aligned}
&e^{2z\tau}-e^{z\tau}+\tau(cc_1\rho_0)^2V'(\rho_0)e^{\alpha\tau z}\left(e^{ik}-1\right)\\
&\quad+\tau[c(1-c_1)\rho_0]^2V'(\rho_0)e^{\alpha\tau z}\left(e^{-ik}-1\right)\\
&\quad+\tau[(1-c)c_2\rho_0]^2V'(\rho_0)e^{\alpha\tau z}\left(e^{ik}-1\right)\\
&\quad+\tau[(1-c)(1-c_2)\rho_0]^2V'(\rho_0)e^{\alpha\tau z}\left(e^{-ik}-1\right)\\
&\quad+\lambda\tau(cc_1\rho_0)^2V'(\rho_0)e^{\alpha\tau z}\left(2e^{ik}-e^{2ik}-1\right)\\
&\quad+\lambda\tau[c(1-c_1)\rho_0]^2V'(\rho_0)e^{\alpha\tau z}\left(2e^{-ik}-e^{-2ik}-1\right)\\
&\quad+\lambda\tau[(1-c)c_2\rho_0]^2V'(\rho_0)e^{\alpha\tau z}\left(2e^{ik}-e^{2ik}-1\right)\\
&\quad+\lambda\tau[(1-c)(1-c_2)\rho_0]^2V'(\rho_0)e^{\alpha\tau z}\\
&\quad\left(2e^{-ik}-e^{-2ik}-1\right)=0,
\end{aligned}\tag{18}$$

where $z=z_1(ik)+z_2(ik)^2+\cdots$ and inserts it into Eq. (18), the first- and second-order terms of ik are obtained

$$\begin{aligned}
z_1&=-h\rho_0^2V'(\rho_0),\\
z_2&=-\frac{3\tau z_1^2}{2}-\frac{f\rho_0^2V'(\rho_0)}{2}-\alpha\tau z_1^2+\lambda f\rho_0^2V'(\rho_0),
\end{aligned}\tag{19}$$

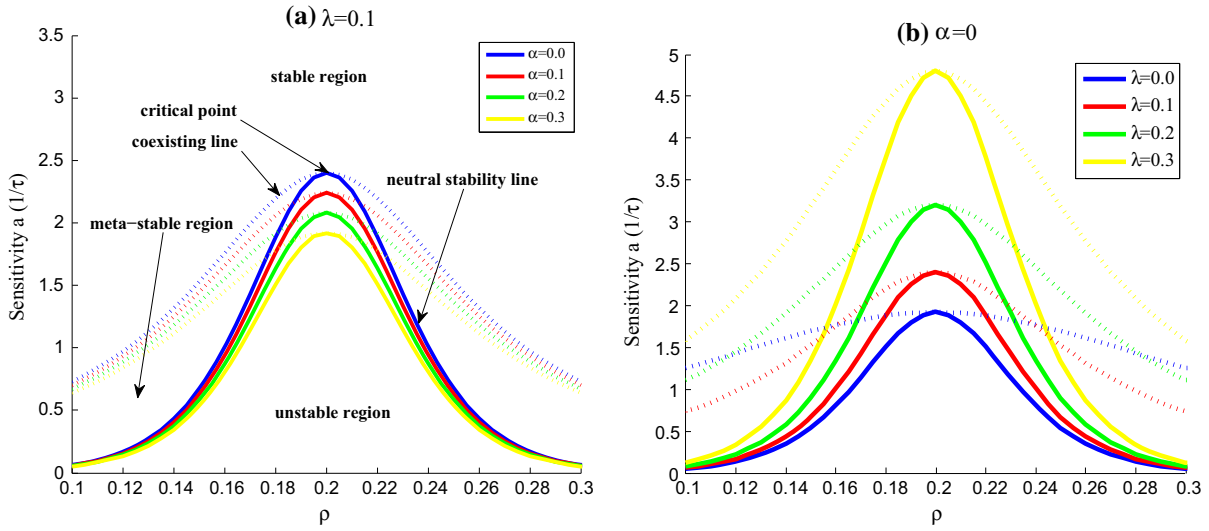

Fig. 2 Phase diagram in the (ρ, a) space with $\rho_0 = \rho_c = 0.2$, $c = c_1 = c_2 = 0.1$ for **a** different values of α; **b** different values of λ.

(20)

where

$$\begin{aligned} f =&(cc_1)^2 + [c(1-c_1)]^2 + [(1-c)c_2]^2 \\ &+ [(1-c)(1-c_2)]^2, \\ h =&(cc_1)^2 - [c(1-c_1)]^2 + [(1-c)c_2]^2 \\ &- [(1-c)(1-c_2)]^2. \end{aligned}$$

If $z_2 > 0$, the uniform steady state becomes stable, while the uniform steady state becomes unstable if $z_2 < 0$. Then the stable condition for pedestrian flow is

$$\tau < \frac{(2\lambda - 1) f}{(3 - 2\alpha) h^2 \rho_0^2 V'(\rho_0)}. \tag{21}$$

Moreover, for small disturbances of long wave length, the neutral stability condition is given by

$$\tau_s = \frac{(2\lambda - 1) f}{(3 - 2\alpha) h^2 \rho_0^2 V'(\rho_0)}. \tag{22}$$

When $c_1 = c_2 = 0.5$, then $h = 0$, there is a singularity irrespective of the value of c, which reflects the phase transition never occurs without the unstable region.

The coexisting curves (dash lines), neutral stability lines (solid lines) and critical points in the space (ρ, a) $(a = 1/\tau)$ for different values of λ and α with $\rho_0 = \rho_c = 0.2$, $c = c_1 = c_2 = 0.1$ are shown in Fig. 2, respectively. The coexisting curve and the neutral stability line are similar to the conventional gas–liquid phase transition. Three regions in the pedestrian flow are distinguished: the unstable region which is within the neutral stability line, the metastable region which is between the neutral stability line, and the coexisting curve and the stable region which is out of the coexisting curve. When $\lambda = 0, \alpha = 0$ in Fig. 2b, it is agreed with the result in Ref. [19]. From Fig. 2a, it is shown that the pedestrian flow becomes stable with the increase of α, which means that pedestrian jam can be suppressed efficiently by enhancing the anticipation of pedestrian. Without the anticipation which as shown in Fig. 2b, the passing effect will aggravate the pedestrian jam with the increasing of λ.

4 Nonlinear analysis

In this section, by using the reductive perturbation method introduced in Ref. [35], we derive the nonlinear equations in the stable, metastable and unstable regions, respectively. We introduce slow scales for space variable j, m and time variable t and define slow variables X and T for $0 < \varepsilon \ll 1$ [44]

$$X = \varepsilon(j + m + bt), \qquad T = \varepsilon^s t \tag{23}$$

where b is a constant to be determined. Assuming

$$\rho(j, m, t) = \rho_0 + \varepsilon^l R(X, T). \tag{24}$$

The values of the index s, l represent different phases of the pedestrian flow. Three groups of values $s = 2, l = 1; s = 3, l = 2; s = 3, l = 1$ are corresponding to the stable pedestrian flow region, metastable pedestrian flow region and unstable pedestrian flow, respectively.

By Substituting Eqs. (23)–(24) into Eq. (14) and expanding to the $s + l + 1$ order of ε, we obtain the following nonlinear partial differential equation

$$\begin{aligned}
&\varepsilon^{l+1}\Big(b + h\rho_0^2 V'(\rho_0)\Big)\partial_X R \\
&+ \varepsilon^{l+2}\Big(\frac{3b^2\tau}{2} + \frac{f + 2bh\alpha\tau + \lambda P_1}{2}\rho_0^2 V'(\rho_0)\Big)\partial_X^2 R \\
&+ \varepsilon^{l+3}\Big(\frac{P_2 + \lambda P_3}{6}\rho_0^2 V'(\rho_0) + \frac{7b^3\tau^2}{6}\Big)\partial_X^3 R \\
&+ \varepsilon^{l+4}\Big(\frac{5b^4\tau^3}{8} + \frac{P_4 + \lambda P_5}{24}\rho_0^2 V'(\rho_0)\Big)\partial_X^4 R \\
&+ \varepsilon^{2l+1}\frac{h}{2}\rho_0^2 V''(\rho_0)\partial_X R^2 \\
&+ \varepsilon^{2l+2}\frac{f + 2bh\alpha\tau + \lambda P_1}{4}\rho_0^2 V''(\rho_0)\partial_X^2 R^2 \\
&+ \varepsilon^{3l+1}\frac{h}{6}\rho_0^2 V'''(\rho_0)\partial_X R^3 \\
&+ \varepsilon^{3l+2}\frac{f + 2bh\alpha\tau + \lambda P_1}{12}\rho_0^2 V'''(\rho_0)\partial_X^2 R^3 \\
&+ \varepsilon^{s+l}\partial_T R + \varepsilon^{s+l+1}(3b\tau \\
&+ h\alpha\tau\rho_0^2 V'(\rho_0))\partial_X\partial_T R = 0. \qquad (25)
\end{aligned}$$

Here

$$\begin{aligned}
P_1 &= (cc_1)^2[2(1 + b\alpha\tau)^2 - (2 + b\alpha\tau)^2 - (b\alpha\tau)^2] \\
&\quad + [c(1 - c_1)]^2[2(-1 + b\alpha\tau)^2 \\
&\quad - (-2 + b\alpha\tau)^2 - (b\alpha\tau)^2] \\
&\quad + [(1 - c)c_2]^2[2(1 + b\alpha\tau)^2 \\
&\quad - (2 + b\alpha\tau)^2 - (b\alpha\tau)^2] \\
&\quad + [(1 - c)(1 - c_2)]^2[2(-1 + b\alpha\tau)^2 \\
&\quad - (-2 + b\alpha\tau)^2 - (b\alpha\tau)^2], \\
P_2 &= (cc_1)^2[(1 + b\alpha\tau)^3 - (b\alpha\tau)^3] \\
&\quad + [c(1 - c_1)]^2[(-1 + b\alpha\tau)^3 - (b\alpha\tau)^3] \\
&\quad + [(1 - c)c_2]^2[(1 + b\alpha\tau)^3 - (b\alpha\tau)^3] \\
&\quad + [(1 - c)(1 - c_2)]^2[(-1 + b\alpha\tau)^3 - (b\alpha\tau)^3], \\
P_3 &= (cc_1)^2[2(1 + b\alpha\tau)^3 - (2 + b\alpha\tau)^3 - (b\alpha\tau)^3] \\
&\quad + [c(1 - c_1)]^2[2(-1 + b\alpha\tau)^3 \\
&\quad - (-2 + b\alpha\tau)^3 - (b\alpha\tau)^3] \\
&\quad + [(1 - c)c_2]^2[2(1 + b\alpha\tau)^3 \\
&\quad - (2 + b\alpha\tau)^3 - (b\alpha\tau)^3] \\
&\quad + [(1 - c)(1 - c_2)]^2[2(-1 + b\alpha\tau)^3 \\
&\quad - (-2 + b\alpha\tau)^3 - (b\alpha\tau)^3], \\
P_4 &= (cc_1)^2[(1 + b\alpha\tau)^4 - (b\alpha\tau)^4] \\
&\quad + [c(1 - c_1)]^2[(-1 + b\alpha\tau)^4 - (b\alpha\tau)^4] \\
&\quad + [(1 - c)c_2]^2[(1 + b\alpha\tau)^4 - (b\alpha\tau)^4] \\
&\quad + [(1 - c)(1 - c_2)]^2[(-1 + b\alpha\tau)^4 - (b\alpha\tau)^4]. \\
P_5 &= (cc_1)^2[2(1 + b\alpha\tau)^4 - (2 + b\alpha\tau)^4 - (b\alpha\tau)^4] \\
&\quad + [c(1 - c_1)]^2[2(-1 + b\alpha\tau)^4 \\
&\quad - (-2 + b\alpha\tau)^4 - (b\alpha\tau)^4] \\
&\quad + [(1 - c)c_2]^2[2(1 + b\alpha\tau)^4 \\
&\quad - (2 + b\alpha\tau)^4 - (b\alpha\tau)^4] \\
&\quad + [(1 - c)(1 - c_2)]^2[2(-1 + b\alpha\tau)^4 \\
&\quad - (-2 + b\alpha\tau)^4 - (b\alpha\tau)^4].
\end{aligned}$$

Firstly, we discuss the triangular shock waves of the pedestrian flow in the stable region. The nonlinear partial differential equation is obtained from Eq. (25) for $s = 2, l = 1$.

$$\begin{aligned}
&\varepsilon^2\Big(b + h\rho_0^2 V'(\rho_0)\Big)\partial_X R \\
&+ \varepsilon^3\Big[\partial_T R + \frac{h}{2}\rho_0^2 V''(\rho_0)\partial_X R^2 + \Big(\frac{3b^2\tau}{2} \qquad (26) \\
&+ \frac{f + 2bh\alpha\tau + \lambda P_1}{2}\rho_0^2 V'(\rho_0)\Big)\partial_X^2 R\Big] = 0.
\end{aligned}$$

Taking $b = -h\rho_0^2 V'(\rho_0)$, the second-order terms of ε are eliminated in Eq. (26). We obtain the following partial differential equation

$$\begin{aligned}
&\partial_T R + h\rho_0^2 V''(\rho_0) R\partial_X R \\
&= \left[\frac{-f - 2bh\alpha\tau - \lambda P_1 - 3h^2\rho_0^2 V'(\rho_0)\tau}{2}\rho_0^2 V'(\rho_0)\right]\partial_X^2 R. \qquad (27)
\end{aligned}$$

In accordance with criterion Eq. (22), the coefficient of the second derivative of Eq. (27) is positive in the stable region. Therefore, in the stable region, Eq. (27) is just the Burgers equation. If $R(X, 0)$ is of compact support, then the solution $R(X, T)$ of Eq. (27) is

$$\begin{aligned}
R(X, T) &= \frac{1}{|h\rho_0^2 V''(\rho_0)|T}\left[X - \frac{\eta_{n+1} + \eta_n}{2}\right] \\
&\quad - \frac{\eta_{n+1} - \eta_n}{2|h\rho_0^2 V''(\rho_0)|T} \\
&\quad \times \tanh\left[\Big(\frac{-f - 2bh\alpha\tau - \lambda P_1 - 3h^2\rho_0^2 V'(\rho_0)\tau}{8}\right. \\
&\quad \left.\rho_0^2 V'(\rho_0)\Big)\frac{(\eta_{n+1} - \eta_n)(X - \xi_n)}{|h\rho_0^2 V''(\rho_0)|T}\right]. \qquad (28)
\end{aligned}$$

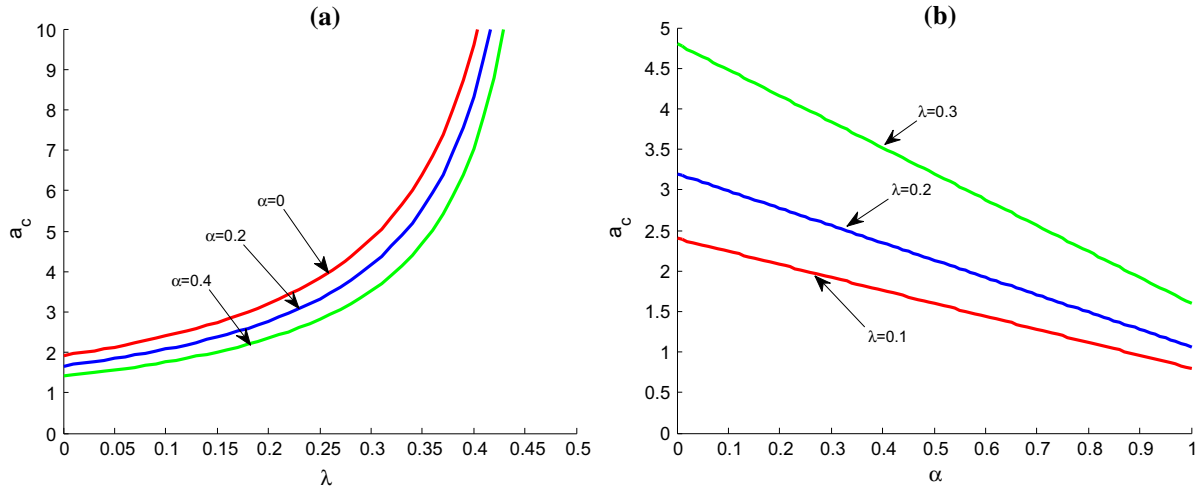

Fig. 3 Plot of a_c with $\rho_0^2 V_0'(\rho_0)|_{\rho_0=\rho_c} = -1, c = c_1 = c_2 = 0.1$ against **a** λ; **b** α.

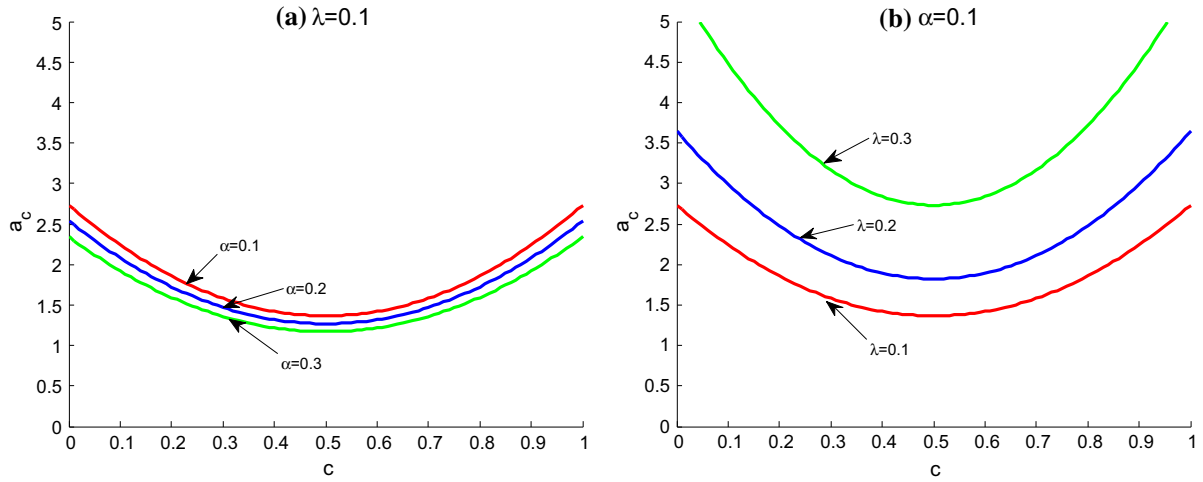

Fig. 4 Plot of a_c against c with $\rho_0^2 V_0'(\rho_0)|_{\rho_0=\rho_c} = -1, c_1 = c_2 = 0.1$ for different values of **a** α; **b** λ.

where ξ_n are the coordinates of the shock fronts and η_n are the coordinates of the intersections of the slopes with the x-axis ($n = 1, 2, ..., N$). As $O(\frac{1}{T})$, $R(X, T)$ decays to 0 when $T \to +\infty$. That means any shock wave expressed by Eq. (28) in stable pedestrian flow region will evolve to a uniform flow when time is sufficiently large.

Secondly, we discuss the soliton waves of the pedestrian flow in the metastable region. The nonlinear partial differential equation is obtained from Eq. (25) for $s = 3, l = 2$.

$$
\begin{aligned}
&\varepsilon^3\Big(b + h\rho_0^2 V'(\rho_0)\Big)\partial_X R \\
&+\varepsilon^4\Big(\frac{3b^2\tau}{2} + \frac{f + 2bh\alpha\tau + \lambda P_1}{2}\rho_0^2 V'(\rho_0)\Big)\partial_X^2 R \\
&+\varepsilon^5\Big[\partial_T R + \frac{h}{2}\rho_0^2 V''(\rho_0)\partial_X R^2 \\
&+\Big(\frac{P_2 + \lambda P_3}{6}\rho_0^2 V'(\rho_0) + \frac{7b^3\tau^2}{6}\Big)\partial_X^3 R\Big] \\
&+\varepsilon^6\Big[\frac{f + 2bh\alpha\tau + \lambda P_1}{4}\rho_0^2 V''(\rho_0)\partial_X^2 R^2 \\
&+(3b\tau + h\alpha\tau\rho_0^2 V'(\rho_0))\partial_X\partial_T R \\
&+\Big(\frac{5b^4\tau^3}{8} + \frac{P_4 + \lambda P_5}{24}\rho_0^2 V'(\rho_0)\Big)\partial_X^4 R\Big] = 0.
\end{aligned}
\tag{29}
$$

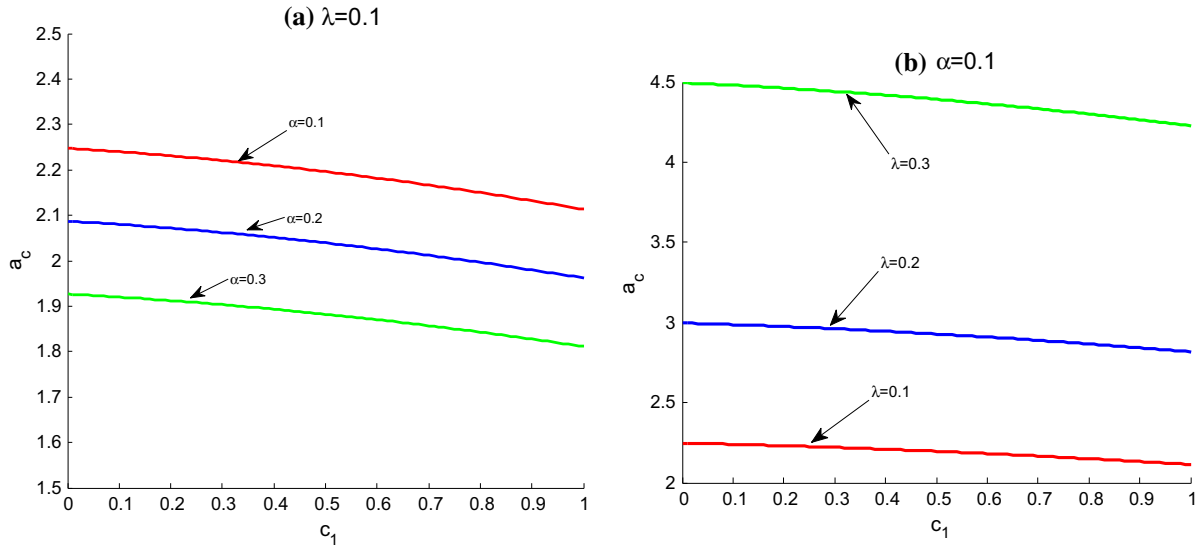

Fig. 5 Plot of a_c against c_1 with $\rho_0^2 V_0'(\rho_0)|_{\rho_0=\rho_c} = -1$, $c = c_2 = 0.1$ for different values of **a** α; **b** λ.

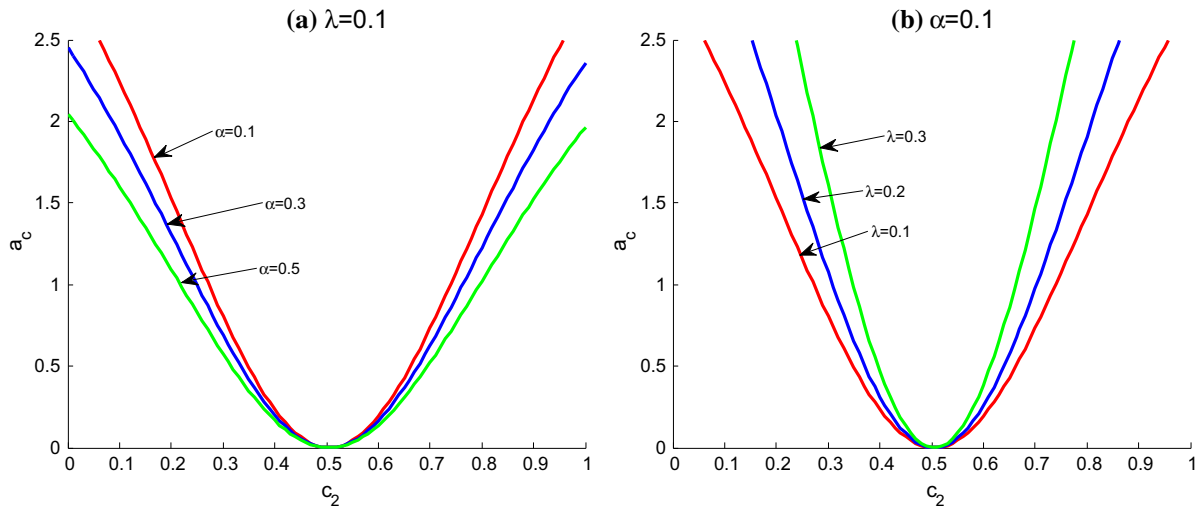

Fig. 6 Plot of a_c against c_2 with $\rho_0^2 V_0'(\rho_0)|_{\rho_0=\rho_c} = -1$, $c = c_2 = 0.1$ for different values of **a** α; **b** λ.

Near the neutral stability line in the unstable region, let

$$\frac{\tau}{\tau_s} = 1 - \varepsilon^2. \tag{30}$$

By taking $b = -h\rho_0^2 V_0'(\rho_0)$, the third- and fourth-order terms of ε are eliminated from Eqs. (29), and Eq. (29) can be rewritten as

$$\begin{aligned} &\varepsilon^5 \left[\partial_T R - f_1 \partial_X^3 R - f_2 R \partial_X R\right] \\ &\quad + \varepsilon^6 \left[-f_3 \partial_X^2 R + f_4 \partial_X^2 R^2 + f_5 \partial_X^4 R\right] = 0 \end{aligned} \tag{31}$$

where

$$\begin{aligned} f_1 &= \left[\frac{7(2\lambda-1)^2 f^2}{6(3-2\alpha)^2 h} - \frac{P_2 + \lambda P_3}{6}\right] \rho_0^2 V'(\rho_0), \\ f_2 &= -h\rho_0^2 V''(\rho_0), \\ f_3 &= -\frac{f + 2bh\alpha\tau + \lambda P_1}{2} \rho_0^2 V'(\rho_0), \\ f_4 &= -\frac{f + 2bh\alpha\tau + \lambda P_1}{4} \rho_0^2 V''(\rho_0), \\ f_5 &= \left[\frac{f(2\lambda-1)(\alpha-3)(P_2+\lambda P_3)}{6h(3-2\alpha)}\right. \end{aligned}$$

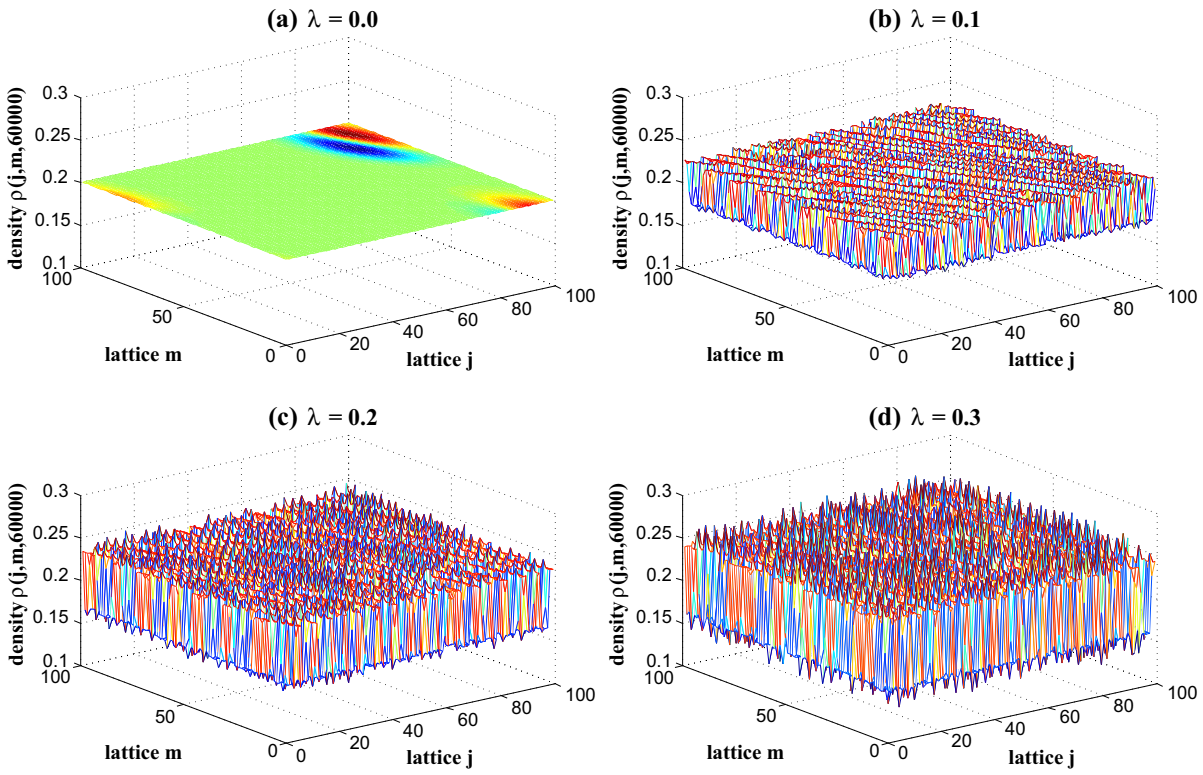

Fig. 7 The pedestrian patterns at time t =60,000 where $a = 2$, $\rho_0 = \rho_c = 0.2$, $c = c_1 = c_2 = 0.1$ for $\lambda = 0, 0.1, 0.2, 0.3$ with $\alpha = 0$, respectively.

$$+\frac{f^3(2\lambda-1)^3(28\alpha-69)}{24h^2(3-2\alpha)^3}-\frac{P_4+\lambda P_5}{24}\Bigg]\rho_0^2V'(\rho_0).$$

In order to derive the standard KdV equation with higher-order correction, we make the following transformation in Eq. (31)

$$T=\sqrt{f_1}T_k,\quad X=-\sqrt{f_1}X_k,\quad R=\frac{1}{f_2}R_k. \tag{32}$$

By using of Eq. (32), we obtain the standard KdV equation with higher-order correction term

$$\partial_{T_k}R_k+\partial^3_{X_k}R_k+R_k\partial_{X_k}R_k +\frac{\varepsilon}{\sqrt{f_1}}\left[-f_3\partial^2_{X_k}R_k+\frac{f_4}{f_2}\partial^2_{X_k}R_k^2+\frac{f_5}{f_1}\partial^4_{X_k}R_k\right]=0. \tag{33}$$

Next, we assume that $R_k(X_k, T_k) = R_0(X_k, T_k) + \varepsilon R_1(X_k, T_k)$ to consider the $O(\varepsilon)$ correction in Eq. (33). If we ignore the $O(\varepsilon)$ term in Eq. (33), it is just the KdV equation with the soliton solution

$$R_0(X_k,T_k)=A\,\mathrm{sech}^2\left[\sqrt{\frac{A}{12}}\left(X_k-\frac{A}{3}T_k\right)\right], \tag{34}$$

where A is a free parameter. It is the amplitude of soliton solutions of the KdV equation. The perturbation term in Eq. (33) gives the condition of selecting a unique member from the continuous family of KdV solitons. In order to obtain the value of A, the solvability condition

$$(R_0, M[R_0]) \equiv \int_{-\infty}^{\infty} \mathrm{d}X_k R_0 M[R_0] = 0 \tag{35}$$

must be satisfied, here $M[R_0]$ is the $O(\varepsilon)$ term in Eq. (33). By computing the integration in Eq. (35), we obtain the value of amplitude A

$$A=\frac{21f_1f_2f_3}{24f_1f_4-5f_2f_5}. \tag{36}$$

Substituting the values of $f_1 - f_5$ into Eq. (36), we get the value of A. Substituting each variable by the original one, we obtain the soliton solution of the density

$$\rho(j,m,t)=\rho_0+\frac{A}{f_2}\left(\frac{\tau}{\tau_s}-1\right)\mathrm{sech}^2$$

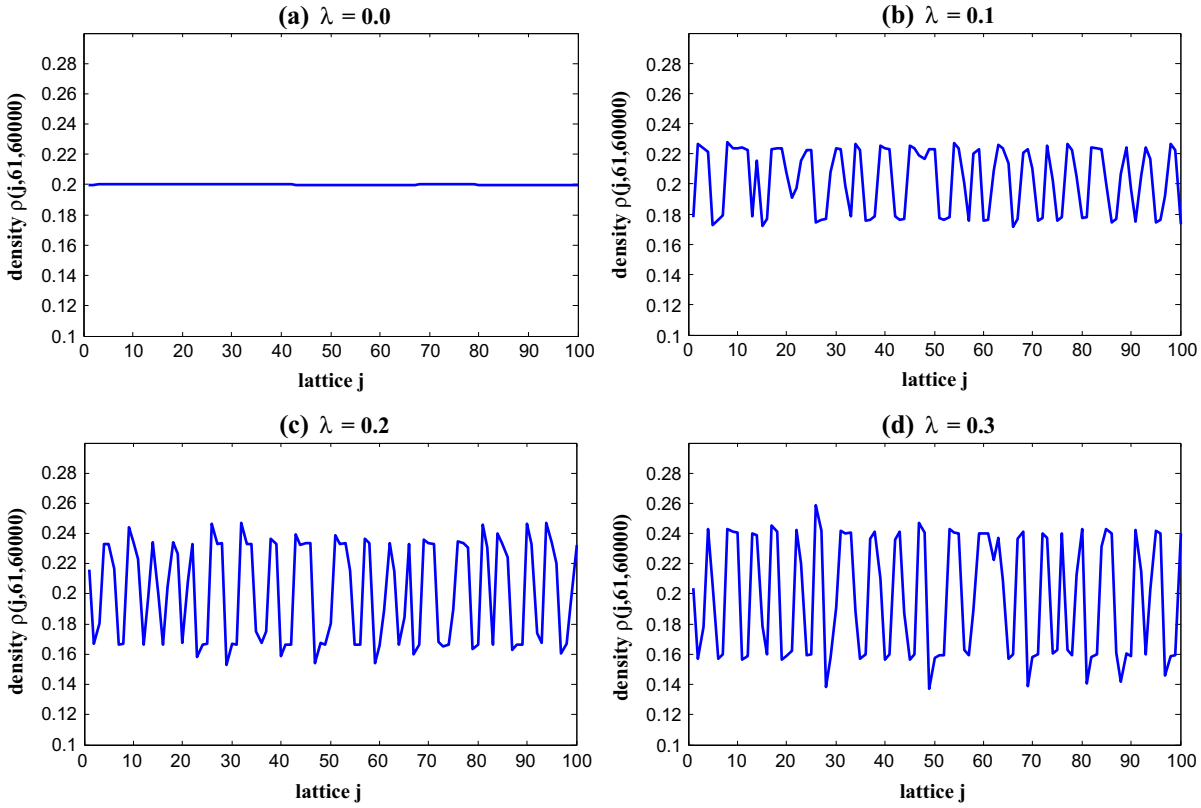

Fig. 8 The density profiles $\rho(j, 60, t)$ at time $t = 60{,}000$ where $a = 2$, $\rho_0 = \rho_c = 0.2$, $c = c_1 = c_2 = 0.1$ for $\lambda = 0, 0.1, 0.2, 0.3$ with $\alpha = 0$, respectively.

$$\left[\sqrt{\frac{A}{12f_1}\left(\frac{\tau}{\tau_s}-1\right)}\left(j+m+\rho_0^2V'(\rho_0)t+\frac{A}{3}\left(\frac{\tau}{\tau_s}-1\right)t\right)\right]. \tag{37}$$

Now, we have derived the soliton density wave described by the KdV equation near the neutral stability line.

Finally, we discuss the kink–antikink waves of the pedestrian flow in the unstable region. The nonlinear partial differential equation is obtained from Eq. (25) for $s = 3, l = 1$.

$$\begin{aligned}&\varepsilon^2\Big(b+h\rho_c^2V'(\rho_c)\Big)\partial_X R\\&+\varepsilon^3\Big(\frac{3b^2\tau}{2}+\frac{f+2bh\alpha\tau+\lambda P_1}{2}\rho_c^2V'(\rho_c)\Big)\partial_X^2R\\&+\varepsilon^4\Big[\Big(\frac{P_2+\lambda P_3}{6}\rho_c^2V'(\rho_c)+\frac{7b^3\tau^2}{6}\Big)\partial_X^3R\\&+\frac{h}{6}\rho_c^2V'''(\rho_c)\partial_X R^3+\partial_T R\Big]\\&+\varepsilon^5\Big[\Big(\frac{5b^4\tau^3}{8}+\frac{P_4+\lambda P_5}{24}\rho_c^2V'(\rho_c)\Big)\partial_X^4R\\&+\frac{f+2bh\alpha\tau+\lambda P_1}{12}\rho_c^2V'''(\rho_c)\partial_X^2R^3\\&+(3b\tau+h\alpha\tau\rho_0^2V'(\rho_0))\partial_X\partial_T R\Big]=0.\end{aligned} \tag{38}$$

Supposing

$$\frac{\tau}{\tau_c}=1+\varepsilon^2 \tag{39}$$

for τ near the critical point $(h_c, 1/\tau_c)$, where $\tau_c = \frac{(2\lambda-1)f}{(3-2\alpha)h^2\rho_c^2V'(\rho_c)}$, the second- and third-order terms of ε can be eliminated from Eq. (38). Then Eq. (38) can be rewritten as

$$\begin{aligned}&\varepsilon^4\Big[\partial_T R-g_1\partial_X^3R+g_2\partial_X R^3\Big]\\&+\varepsilon^5\Big[g_3\partial_X^2R+g_4\partial_X^2R^3+g_5\partial_X^4R\Big]=0\end{aligned} \tag{40}$$

where

$$g_1=\left[\frac{7(2\lambda-1)^2f^2}{6(3-2\alpha)^2h}-\frac{P_2+\lambda P_3}{6}\right]\rho_c^2V'(\rho_c),$$

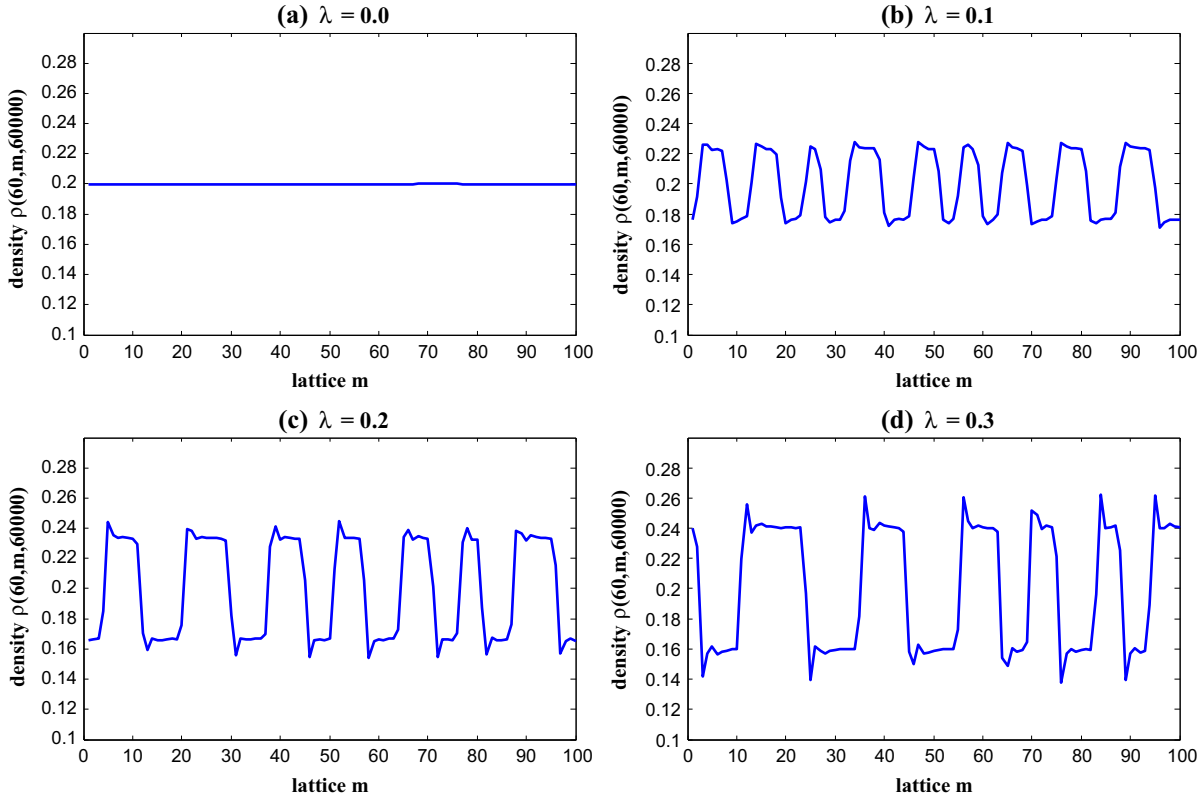

Fig. 9 The density profiles $\rho(60, m, t)$ at time $t = 60,000$ where $a = 2$, $\rho_0 = \rho_c = 0.2$, $c = c_1 = c_2 = 0.1$ for $\lambda = 0, 0.1, 0.2, 0.3$ with $\alpha = 0$, respectively.

$$g_2 = -\frac{h}{6}\rho_c^2 V'''(\rho_c),$$
$$g_3 = -\frac{f + 2bh\alpha\tau + \lambda P_1}{2}\rho_c^2 V'(\rho_c),$$
$$g_4 = -\frac{f + 2bh\alpha\tau + \lambda P_1}{12}\rho_c^2 V'''(\rho_c),$$
$$g_5 = \left[\frac{f(2\lambda-1)(\alpha-3)(P_2+\lambda P_3)}{6h(3-2\alpha)} + \frac{f^3(2\lambda-1)^3(28\alpha-69)}{24h^2(3-2\alpha)^3} - \frac{P_4+\lambda P_5}{24}\right]\rho_c^2 V'(\rho_c).$$

In order to derive the standard MKdV equation with higher-order correction, we make the following transformation in Eq. (40)

$$T = \frac{1}{g_1}T_m, \quad R = \sqrt{\frac{g_1}{g_2}}R_m. \tag{41}$$

Then we obtain the standard MKdV equation with higher-order correction term

$$\partial_{T_m} R_m - \partial_X^3 R_m + \partial_X R_m^3 + \frac{\varepsilon}{g_1}\left[g_3\partial_X^2 R_m + \frac{g_1 g_4}{g_2}\partial_X^2 R_m^3 + g_5\partial_X^4 R_m\right] = 0. \tag{42}$$

If we ignore the $O(\varepsilon)$ term in Eq. (42), it is just the MKdV equation with the kink–antikink solution

$$R_{m0}(X, T_m) = \sqrt{B}\tanh\sqrt{\frac{B}{2}}(X - BT_m). \tag{43}$$

Similar to the process of deriving the amplitude A for KdV equation, we obtain the value of propagation velocity B for the kink–antikink solution as follows

$$B = \frac{5g_2 g_3}{2g_2 g_5 - 3g_1 g_4} \tag{44}$$

which is the same as the one in Ref. [33]. Inserting Eq. (41) into Eq. (43), we get the solution of the MKdV equation

$$R(X, T) = \sqrt{\frac{g_1 B}{g_2}}\tanh\sqrt{\frac{B}{2}}(X - Bg_1 T). \tag{45}$$

Then we gain the kink–antikink solution of the density

$$\rho(j, m, t) = \rho_c + \sqrt{\frac{g_1 B}{g_2}\left(\frac{\tau}{\tau_c} - 1\right)}\tanh$$

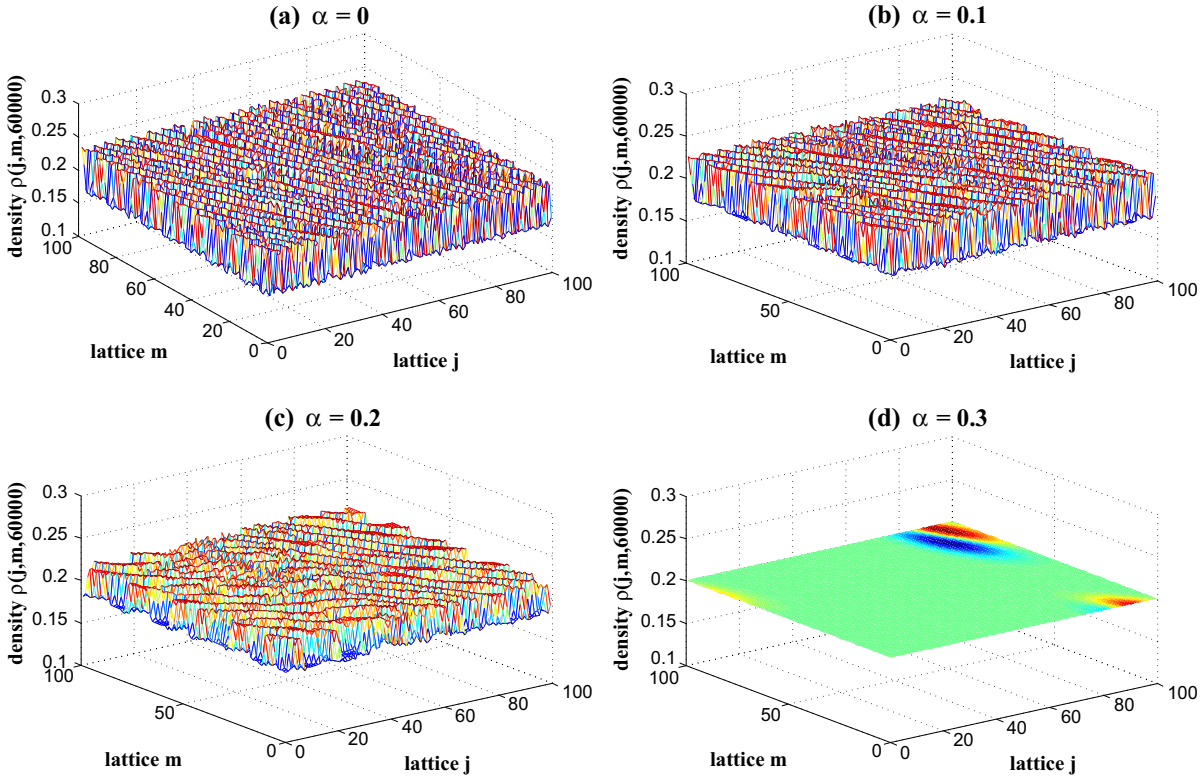

Fig. 10 The pedestrian patterns at time t =60,000 where $a = 1.9$, $\rho_0 = \rho_c = 0.2$, $c = c_1 = c_2 = 0.1$ for $\alpha = 0, 0.1, 0.2, 0.3$ with $\lambda = 0.1$, respectively.

$$\times \left[\sqrt{\frac{B}{2}\left(\frac{\tau}{\tau_c}-1\right)}\left(j+m+\rho_c^2 V'(\rho_c)t - Bg_1\left(\frac{\tau}{\tau_c}-1\right)t\right)\right]. \quad (46)$$

And the amplitude C of the kink–antikink solution equation (46) is given by

$$C = \sqrt{\frac{g_1 B}{g_2}\left(\frac{\tau}{\tau_c}-1\right)}.$$

The kink solution represents the coexisting phase, which consists of the freely moving phase with low density and the congested phase with high density. The coexisting curve can be described by $\rho = \rho_c \pm C$. Therefore, we get the coexisting curve in the (ρ, a) plane (see Fig. 2).

5 Simulation

To check the theoretical results, we carry out numerical simulations in this section. The initial conditions of the numerical simulation are as follows: There are $N = 100$ lattices in the system, and the periodical boundary condition is applied. The initial perturbations are adopted as follows: $\rho(j, m, 0) = \rho_0 = \rho_c = 0.2$. The local densities $\rho(N/2, N/2, 1)$ and $\rho(N/2-1, N/2-1, 1)$ at sites $(N/2, N/2)$ and $(N/2-1, N/2-1)$ at time $t = 1$ are set as 0.15 and 0.25.

Figure 3 shows the plots of a_c against reaction coefficient α and λ, respectively, with $\rho_c^2 V_0'(\rho_c) = -1$, $c = c_1 = c_2 = 0.1$. From Fig. 3a, we can see that the critical sensitivity a_c increases with the increase of λ, which means the pedestrian flow becomes more and more unstable under passing behavior, but the conscious passing behavior (represented by anticipation and its coefficient α) will alleviate the congestion. From Fig. 3b, we can see that the critical sensitivity a_c decreases with the increase of α, which means the pedestrian flow becomes more and more stable under conscious walking behavior.

Figures 4, 5 and 6 show the plots of a_c against c, c_1 and c_2 for different values of α, λ with $\rho_c^2 V_0'(\rho_c) = -1$,

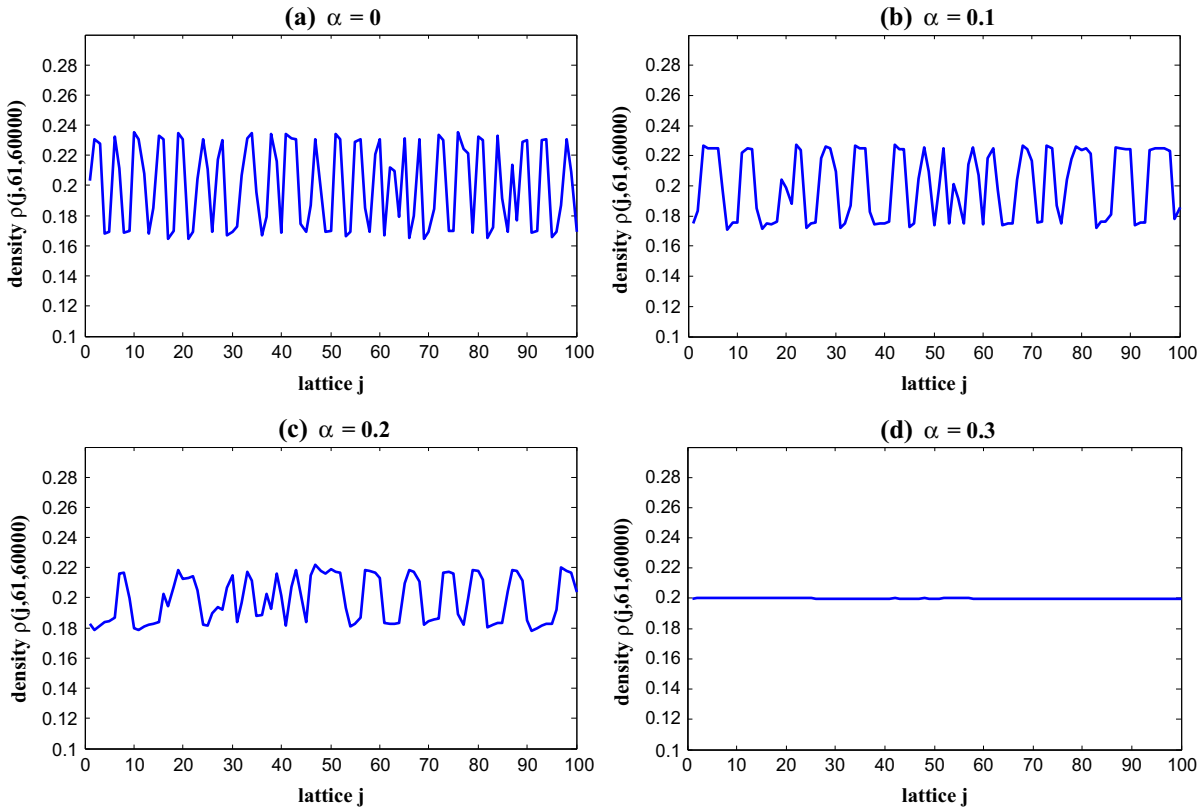

Fig. 11 The density profiles $\rho(j, 60, t)$ at time $t = 60,000$ where $a = 1.9$, $\rho_0 = \rho_c = 0.2$, $c = c_1 = c_2 = 0.1$ for $\alpha = 0, 0.1, 0.2, 0.3$ with $\lambda = 0.1$, respectively.

respectively. From Figs. 4 and 6, the critical sensitivity a_c decreases with the increase of c and c_2 as c, $c_2 \leq 0.5$, and increases with the increase of c and c_2 as $1 \geq c$, $c_2 \geq 0.5$. Figure 5 shows that with the increase of c_1, the critical sensitivity a_c decreases. According to the above results, when c and c_2 remain unchanged, enlarging the east-bound density (c_2) may alleviate the occurrence of jams effectively. From Figs. 4, 5 and 6, we can also see that anticipation and passing effect play an important role in pedestrian flow, which is same with the result in Fig. 2.

Figure 7 shows the pedestrian patterns after a sufficiently long time $t = 60,000$ with different λ for $a = 2$, $\rho_0 = \rho_c = 0.2$, $c = c_1 = c_2 = 0.1$, $\alpha = 0$. In Fig. 7, the patterns (a), (b), (c) and (d) exhibit the time evolution of the density $\rho(j, m, t)$ for $\lambda = 0.0, 0.1, 0.2, 0.3$, respectively. The value of parameter λ is chosen to show the passing effect upon the pedestrian flow. By using the linear stability condition (21), the pedestrian flow is linear unstable in patterns (b), (c) and (d). The pedestrian flow is stable in pattern (a). So the small disturbances will be amplified, and the density waves appear in patterns (b), (c) and (d). The small disturbances dissipate in pattern (a) as time goes on.

Figures 8 and 9 show the density profile obtained at $t = 60,000$ corresponding to Fig. 7, respectively. And it makes us see the evolution of the density with the small disturbances more clearly.

From Figs. 7, 8 and 9, we can see the unconscious passing behavior will make the pedestrian flow become unstable, and the pedestrian jams appear with the passing behavior.

Figure 10 shows the pedestrian patterns after a sufficiently long time $t = 60,000$ with different λ for $a = 1.9$, $\rho_0 = \rho_c = 0.2$, $c = c_1 = c_2 = 0.1$, $\lambda = 0.1$. In Fig. 10, the patterns (a), (b), (c) and (d) exhibit the time evolution of the density $\rho(j, m, t)$ for $\alpha = 0.0, 0.1, 0.2, 0.3$, respectively. The value of parameter α is chosen to show the effect of anticipation upon the pedestrian flow. By using the linear stability condition

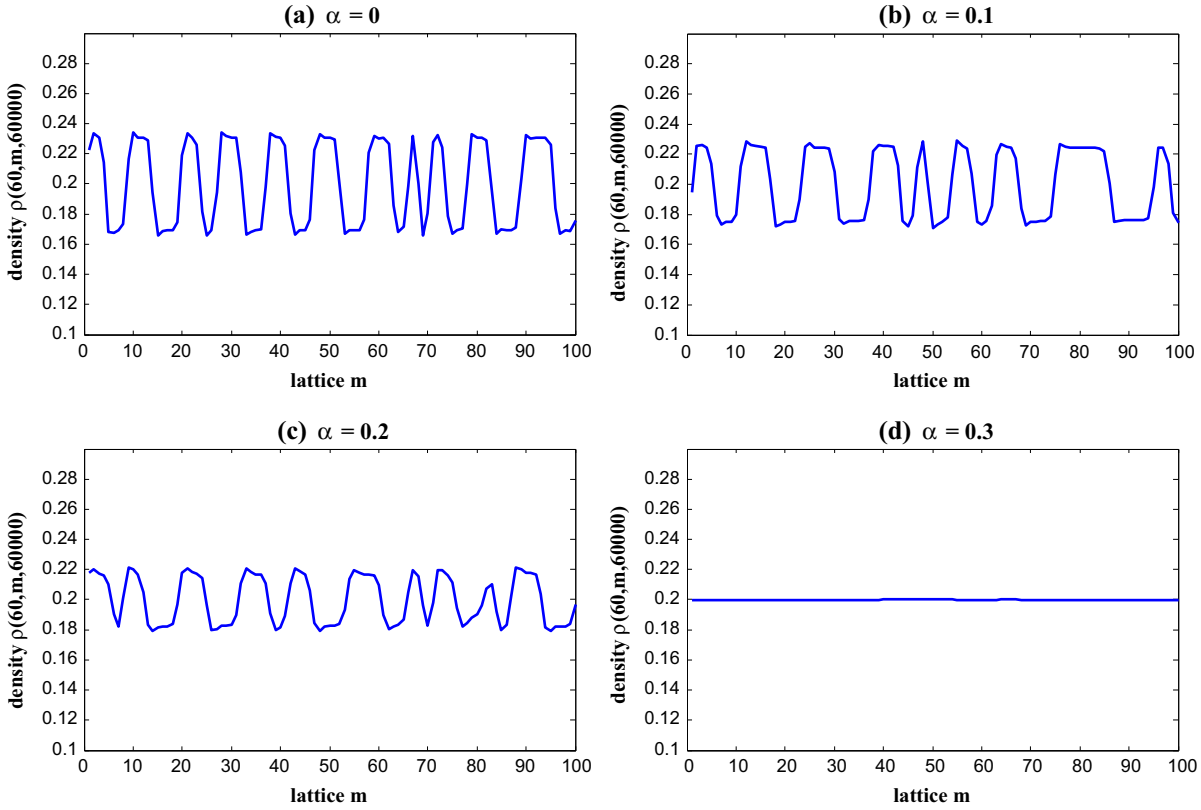

Fig. 12 The density profiles $\rho(60, m, t)$ at time $t = 60,000$ where $a = 1.9$, $\rho_0 = \rho_c = 0.2$, $c = c_1 = c_2 = 0.1$ for $\alpha = 0, 0.1, 0.2, 0.3$ with $\lambda = 0.1$, respectively.

(21), the pedestrian flow is linear unstable in patterns (a), (b) and (c). The pedestrian flow is stable in pattern (d). So the small disturbances will be amplified, and the density waves appear in patterns (a), (b) and (c). The small disturbances dissipate in pattern (d) as time goes on. Figures 11 and 12 show the density profile obtained at $t = 60,000$ corresponding to Fig. 10, respectively.

From Figs. 10, 11 and 12, we can see the pedestrian flow becomes more and more stable with the increasing of α, which means pedestrian jams induced by passing behavior can be alleviated with the consideration of the anticipation effect.

6 Summary

In order to investigate the effect of pedestrian's anticipation upon pedestrian flow, we propose an extended lattice hydrodynamic model for bidirectional pedestrian flow with passing by taking this factor into account. We obtain the stability condition of the proposed model by the use of linear stability theory. The stability condition shows that the anticipation effect plays an important role in influencing the stability of pedestrian flow. The Burgers, KdV and MKdV equations are obtained to describe the pedestrian flow behavior in the stable, metastable and unstable region, respectively. The results show that enlarging the reaction coefficient of pedestrian's anticipation may lead to the stabilization of the pedestrian flow. Such findings indicate that in crowded environment such as railway entrance and the corner of subway tunnel, pedestrian should enhance awareness of walking behavior and try to avoid passing behavior in order to make the pedestrian flow stable. The numerical simulations show a good agreement with the analytical results.

Acknowledgments The authors wish to thank the anonymous referees for their useful comments. This work was partially supported by the National Natural Science Foundation of China (Grant No. 61134004), Zhejiang Province National Science

Foundation (Grant No. LY12A010 09) and Zhejiang Province Educational Research Project(Grant No. Y2013 28023).

References

1. Helbing, D.: Traffic and related self-driven many-particle systems. Rev. Mod. Phys. **73**(4), 1067–1141 (2001)
2. Nagatani, T.: The physics of traffic jams. Rep. Prog. Phys. **65**, 1331–1386 (2002)
3. Helbing, D., Buzna, L., Johansson, A., Werner, T.: Selforganized pedestrian crowd dynamics: experiments, simulations, and design solutions. Transp. Sci. **39**, 1–24 (2005)
4. Waldau, N., Gattermann, P., Knoflacher, H., Schreckenberg, M.: Pedestrian and Evacuation Dynamic 2005. Springer, Berlin (2007)
5. Robin, T., Antonini, G., Bierlaire, M., Cruz, J.: Specification, estimation and validation of a pedestrian walking behavior model. Transp. Res. B **43**, 36–56 (2009)
6. Schadschneider, A., Chowdhury, D., Nishinari, K.: Stochastic Transport in Complex Systems—From Molecules to Vehicles. Elsevier, Amsterdam (2010)
7. Helbing, D., Farkas, I.J., Vicsek, T.: Simulating dynamical features of escape panic. Nature **407**, 487–490 (2000)
8. Helbing, D., Farkas, I.J., Vicsek, T.: Freezing by heating in a driven mesoscopic system. Phys. Rev. Lett. **84**, 1240–1243 (2000)
9. Helbing, D., Johansson, A., Al-Abideen, H.Z.: Dynamics of crowd disasters: an empirical study. Phys. Rev. E **75**, 046109 (2007)
10. Yu, W., Johansson, A.: Modeling crowd turbulence by many-particle simulations. Phys. Rev. E **76**, 046105 (2007)
11. Helbing, D., Molnr, P.: Social force model for pedestrian dynamics. Phys. Rev. E **51**, 4282–4286 (1995)
12. Johansson, A.: Constant-net-time headway as a key mechanism behind pedestrian flow dynamics. Phys. Rev. E **80**, 026120 (2009)
13. Kuang, H., Chen, T., Li, X.L., Lo, S.M.: A new lattice hydrodynamic model for bidirectional pedestrian flow considering the visual field effect. Nonlinear Dyn. (2013). doi:10.1007/s11071-014-1559-y
14. Tang, T.Q., Huang, H.J., Shang, H.Y.: A new pedestrian-following model for aircraft boarding and numerical tests. Nonlinear Dyn. **67**(1), 437–443 (2012)
15. Xia, Y.H., Wong, S.C., Shu, C.W.: Dynamic continuum pedestrian flow model with memory effect. Phys. Rev. E **79**, 066113 (2009)
16. Burstedde, C., Klauck, K., Schadschneider, A., Zittartz, J.: Simulation of pedestrian dynamics using a two-dimensional cellular automaton. Phys. A **295**, 507–525 (2001)
17. Ezaki, T., Yanagisawa, D., Nishinari, K.: Pedestrian flow through multiple bottlenecks. Phys. Rev. E **86**, 026118 (2012)
18. Zhang, P., Jian, X.X., Wong, S.C., Choi, K.: Potential field cellular automata model for pedestrian flow. Phys. Rev. E **85**, 021119 (2012)
19. Tian, H.H., He, H.D., Wei, Y.F., Xue, Y., Lu, W.Z.: Lattice hydrodynamic model with bidirectional pedestrian flow. Phys. A **388**, 2895–2902 (2009)
20. Anderson, R.W.G., Long, A.D., Serre, T.: Phenomenological continuous contact-impact modelling for multibody simulations of pedestrian–vehicle contact interactions based on experimental data. Nonlinear Dyn. **58**(1–2), 199–208 (2009)
21. McRobie, A.: Nonlinear dynamics of mechanical systems under complicated forcing. Nonlinear Dyn. **43**(1–2), 127–136 (2006)
22. Ivancevic, V.G., Reid, D.J., Aidman, E.V.: Crowd behavior dynamics: entropic path-integral model. Nonlinear Dyn. **59**(1–2), 351–373 (2010)
23. Ivancevic, V.G., Reid, D.J.: Turbulence and shock-waves in crowd dynamics. Nonlinear Dyn. **68**(1–2), 285–304 (2012)
24. Xu, X.L., Chen, Z.Q., Si, G.Y., Hu, X.F., Jiang, Y.Q., Xu, X.S.: The chaotic dynamics of the social behavior selection networks in crowd simulation. Nonlinear Dyn. **64**(1–2), 117–126 (2011)
25. Nagatani, T.: Jamming transition in a two-dimensional traffic flow model. Phys. Rev. E **59**, 4857–4864 (1999)
26. Nagatani, T., Nakanishi, K.: Delay effect on phase transitions in traffic dynamics. Phys. Rev. E **57**(6), 6415–6421 (1998)
27. Nakayama, A., Hasebe, A., Sugiyama, Y.: Instability of pedestrian flow and phase structure in a two-dimensional optimal velocity model. Phys. Rev. E **71**, 036121 (2005)
28. Nakayama, A., Hasebe, A., Sugiyama, Y.: Instability of pedestrian flow in 2D optimal velocity model with attractive interaction. Comput. Phys. Commun. **177**, 162–163 (2007)
29. Yuen, J.K.K., Lee, E.W.M.: The effect of overtaking behavior on unidirectional pedestrian flow. Saf. Sci. **50**, 1704–1714 (2012)
30. Tang, T.Q., Huang, H.J., Shang, H.Y.: A new pedestrian-following model for aircraft boarding and numerical tests. Nonlinear Dyn. **67**, 437–443 (2012)
31. Ivancevic, V.G., Reid, D.J., Aidman, E.V.: Crowd behavior dynamics: entropic path-integral model. Nonlinear Dyn. **59**, 351–373 (2010)
32. Hanseler, F.S., Bierlaire, M., Farooq, B., Muhlematter, T.: A macroscopic loading model for time-varying pedestrian flows in public walking areas. Trans. Res. B **69**, 60–80 (2014)
33. Kerner, B.S., Konhauser, P.: Cluster effect in initially homogeneous traffic flow. Phys. Rev. E **48**(4), 2335–2338 (1993)
34. Kurtze, D.A., Hong, D.C.: Traffic jams, granular flow, and soliton selection. Phys. Rev. E **52**(1), 218–221 (1995)
35. Komatsu, T., Sasa, S.: Kink soliton characterizing traffic congestion. Phys. Rev. E **52**(5), 5574–5582 (1995)
36. Ge, H.X., Cheng, R.J., Dai, S.Q.: KdV and kink–antikink solitons in car-following models. Phys. A **357**, 466–476 (2005)
37. Ngoduy, D.: Effect of driver behaviours on the formation and dissipation of traffic flow instabilities. Nonlinear Dyn. **69**(3), 969–975 (2012)
38. Tang, T.Q., Wang, Y.P., Yang, X.B., Wu, Y.H.: A new car-following model accounting for varying road condition. Nonlinear Dyn. **70**(2), 1397–1405 (2012)
39. Zheng, L.J., Tian, C., Sun, D.H., Liu, W.N.: A new car-following model with consideration of anticipation driving behavior. Nonlinear Dyn. **70**(2), 1205–1211 (2012)
40. Zhu, W.X., Zhang, L.D.: Friction coefficient and radius of curvature effects upon traffic flow on a curved Road. Phys. A **391**, 4597–4605 (2012)

41. Wang, T., Gao, Z.Y., Zhang, J.: Stabilization effect of multiple density difference in the lattice hydrodynamic model. Nonlinear Dyn. **73**, 2197–2205 (2013)
42. Suma, Y., Yanagisawa, D., Nishinari, K.: Anticipation effect in pedestrian dynamics: modeling and experiments. Phys. A **391**, 248–263 (2012)
43. Nagatani, T.: Chaotic jam and phase transition in traffic flow with passing. Phys. Rev. E **60**, 1535–1541 (1999)
44. Cross, M.C., Hohenberg, P.C.: Pattern formation outside of equilibrium. Rev. Mod. Phys. **65**, 851–1112 (1993)